Beyond Thermal Interaction between Ocean and Atmosphere: On the Extratropical Climate Variability due to the Wind-Induced SST*

DONG EUN LEE, ZHENGYU LIU, AND YUN LIU

Center for Climate Research, University of Wisconsin—Madison, Madison, Wisconsin

(Manuscript received 8 June 2006, in final form 20 August 2007)

ABSTRACT

Prescribing sea surface temperature (SST) for the atmospheric general circulation models (GCM) may not lead to underestimation of the coupled variability. In this study, a set of SST-driven atmospheric GCM experiments, starting from slightly different multiple initial conditions, is performed. The SST used here is prepared by a coupled GCM, which has the same atmospheric GCM component as the AGCM used in the experiment with the prescribed SST. The results indicate that prescribing SST leads to underestimation of the coupled air temperature variance only in subtropics. Meanwhile, in midlatitudes, prescribing SST may result in the overestimation of the coupled air temperature variance, where the major role of ocean–atmosphere contrast is to provide damping for SST.

The simple stochastically driven coupled model is revisited with an extension to the direct wind-driven forcing for SST. In addition to the previous setup relying exclusively on the stochastic perturbation for air temperature, the ocean temperature is also forced by the pure random wind. By this extended model, it is speculated that the coupled air temperature variance can be overestimated by prescribing SST, depending on the sensitivity of SST to the wind-driven heat flux. The midlatitude is the most probable place for the overestimation since the wind-driven ocean dynamics can enhance the wind-driven surface heat flux due to the dominant zonal wind anomaly.

1. Introduction

The disaccord of the Atmospheric Model Intercomparison Project (AMIP; Gates 1992)-type simulations, with the observed climate variability, has often been attributed to the lack of coupling with the slowlyresponding ocean. Barsugli and Battisti (1998, hereafter BB98) have provided theoretical background and have demonstrated that low-frequency atmospheric variability at frequencies beyond interannual or lower in the extratropics cannot be conserved by prescribing SST (Barsugli 1995; BB98). According to BB98, the AMIP-type approach fails owing to a lack of the coupled adjustment to the atmospheric internal variability, which is often referred to as "reduced thermal damping." From this view of a thermally coupled climate, it has been commonly believed that the role of an extratropical ocean in the coupled climate system is to amplify the atmospheric signal at low frequencies.

While many atmospheric general circulation model (AGCM) studies broadly apply this concept in interpreting their results (Kushnir et al. 2002), the actual validity of the BB98 simple model for representing the current coupled climate system has not been carefully revisited using GCMs. The previous studies using an AGCM seem to find much agreement with BB98 in their comparison between the pure internal variability and the variability interacting with SSTs (Manabe and Stoffer 1996; Bladé 1997; Bhatt et al. 1998; Saravanan 1998; Saravanan and Chang 1999). However, the major contrast between the two-way interaction and the SST-to-atmosphere interaction has been only partially examined by ignoring a few important caveats to be reconsidered.

First, many AMIP-type simulations find a reduction in variance and improvement in prediction skills in their ensemble mean simulation compared to the observed record (Mehta et al. 2000; Rodwell et al. 1999).

* Center for Climatic Research, University of Wisconsin—Madison Contribution Number 938.

Corresponding author address: Dong Eun Lee, IRI, Earth Institute, Columbia University, Lamont Campus, 61 Route 9W, Monell Building, Rm. 202A, Palisades, NY 10964.
E-mail: dlee@iri.columbia.edu

DOI: 10.1175/2007JCLI1532.1

As seen by Bretherton and Battisti (2000) using the BB98 model, this tendency is also understood as the result of *reduced thermal damping*. However, in AGCM studies, it is not clear how much of the disaccord is due to the model deficiency rather than the inaccurate coupling scheme. Although it is quite obvious that the ensemble mean approach reduces the AGCM variances by lowering the noise level (Bretherton and Battisti 2000; Mehta et al. 2000), it is less convincing that the same GCM coupled with the ocean would generate a larger variance than that of an AGCM, especially when the model deficiency is not removed.

Second, the viewpoint that considers the ocean as a passive heat capacitor was projected onto the interpretation of GCM simulations, which include the full ocean dynamics. The previous studies with GCMs (Bladé 1997, 1999) have reendorsed BB98's interpretation by showing the enhancement of climate variability due to coupling of an AGCM to a slab ocean mixed layer. The impact of the interaction between atmospheric dynamics and SST still remains unclear since their ocean models did not include the ocean dynamics to which the forcing for SST in the midlatitudes has been attributed most dominantly (Namias 1965; Davis 1976). It is a bit ambiguous how a SST without a direct forcing mechanism could achieve the agreement to GCMs, which are devised with the most realistic ocean–atmosphere (O–A) coupling schemes. Indeed, as shown by other studies, SST models with oceanic processes associated with the surface wind (Liu 1993; Saravanan and McWilliams 1998; Seager et al. 2000; Pierce et al. 2001; Dommenget and Latif 2002; Schneider et al. 2002; Czaja et al. 2003; Lee 2006) can better explain the observed records.

Therefore, to fully understand the coupled variability in extratropics, two efforts must be integrated to minimize the gap between GCMs and conceptual models. First, the direct stochastic forcing for ocean induced by local wind should be taken into account as an extension of the conventional stochastically driven climate model (BB98). Second, an AMIP-type experiment must be performed with a prescribed SST generated by the same GCM coupled to ocean. Additionally, the ocean model must include at least the heat flux delivered by Ekman drift for the sake of the essential representation of extratropical O–A interaction. In this way, it is possible to minimize substantially the largest source of uncertainty due to the model deficiency in other AMIP-type studies for hindcasting the observed climate.

In the first half of this report, we repeat BB98's approach using our GCMs. The SSTs simulated by coupled GCMs (CGCMs) are prescribed as boundary conditions for the AGCM simulation. Then, the variances of air temperatures and O–A contrasts are calculated and the CGCM and AGCM results are compared. In the later half, we advance the framework of BB98 and improve the representation of extratropical coupled climate by adding direct wind-induced forcing on SST. In the realistic parameter regime of the wind-induced forcing, we show that enhancement due to coupling explained by "reduced thermal damping" may not be an accurate interpretation in midlatitudes.

2. Design of GCM experiments

Using full GCMs we perform a closer examination of the theoretical insight in a more realistic climate system. We utilized the Fast Ocean–Atmosphere Model (FOAM; Jacob 1997) for this study. The full description can be found in Jacob (1997) and Wu et al. (2003).

The numerical experiment consists of two steps. First, in order to generate the "truth," a fully coupled control run for 50 years is performed and the monthly mean variables are stored (hereafter, COUP). The monthly mean SSTs are stored for boundary conditions in the later experiments as well. This simulation starts after a longer than 700-yr spinup control run. Next, the 50-yr monthly mean SST from this COUP result is prescribed as the boundary condition to force the atmospheric component, starting from nine different initial conditions (hereafter, AMIP). Each initial condition, at least three years apart, is randomly chosen in the control simulation beyond the first 50 years in which the forcing is selected. Anomalies are obtained by subtracting the 50-yr term-mean seasonal cycle from the whole data. In this study, only the anomalies from boreal winter [November–April (NDJFMA)] averages are discussed. A companion experiment using the AMIP approach with climatological SST reproduces almost perfectly the seasonal climatology of the COUP in the entire atmosphere column, with the air temperature differences in the upper troposphere of less than a few tenths of a degree (not shown).

3. Twin experiment: Evidence found disagreeing with BB98

In Fig. 1, the ratios of North Pacific AMIP variance to the coupled variance for winter-mean air temperature at the surface level are presented as a function of location. For AMIP variance, all nine simulations are used. It is shown that COUP variance is larger than AMIP variance in the subtropics, as expected in BB98. However, COUP variance does not significantly exceed the AMIP variance in midlatitudes. This is also true at longer running mean averages (not shown). By an f test,

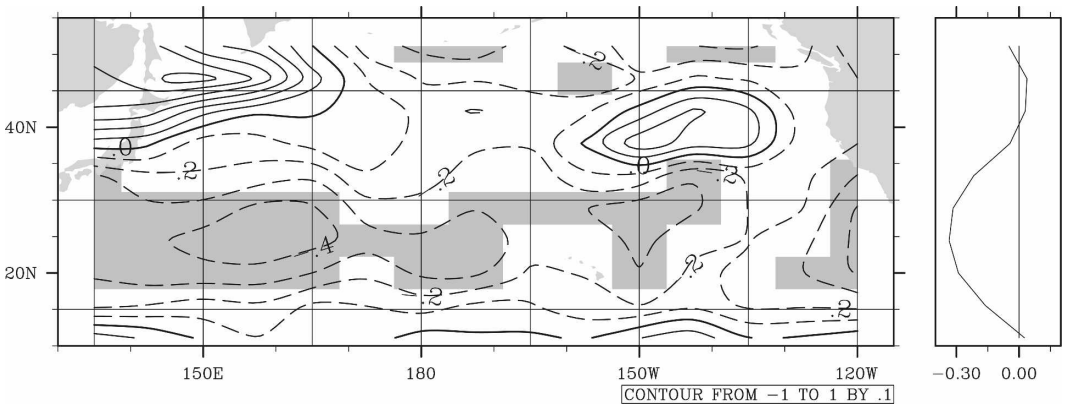

FIG. 1. Deviation of AMIP-to-COUP variance ratio from 1, $\sigma^2(T_a^M)/\sigma^2(T_a^C) - 1$ for the surface air temperature. For the calculation of $\sigma^2(T^M)$, all nine simulations are strung together. Northern winter (November–April) average is used. Shaded in gray, if BB98's hypothesis [H_o: $\sigma^2(T_a^M)/\sigma^2(T_a^C) < 1$] is accepted with 95% significance by an f test.

the BB98 hypothesis of *enhanced variability* due to *coupling* is accepted at 95% significance only in the subtropics. The air temperatures of both the COUP and AMIP maintain roughly the Gaussian distribution. Considering that the model deficiency is minimized by prescribing CGCM-generated SST, this result leads us to raise a fundamental question on the role of thermal coupling between ocean and atmosphere in the extratropical coupled climate system.

To investigate more closely the thermal coupling in the model climate, we compare the O–A contrast of temperature in both simulations. In Fig. 2a, the correlation coefficients of O–A contrast between COUP and ensemble mean AMIP are presented. Monthly means of northern winter months (NDJFMA) are used. In midlatitudes, the correlation coefficients of O–A contrast between the two simulations are most strongly positive (>0.5). This is the same location where the air temperature variance in COUP is not significantly larger than that in AMIP (Fig. 2b). Meanwhile, in the subtropics, the correlation coefficients are close to zero or negative, agreeing with the previous view (BB98; Bretherton and Battisti 2000). There are clear latitudinal preferences for the location of strong positive correlation. The strong positive correlation coefficients in midlatitudes may imply that the role of static forcing due to O–A contrast is in less agreement with BB98, while it is more consistent with BB98 in the subtropics. Even if it is fully granted that the monthly average suppresses the higher-frequency variability, it is not obvious why the stronger positive correlation coefficients appear in midlatitudes.

As shown in Fig. 2b, the variance of coupled O–A contrast does not always appear weaker than that of the ensemble mean AMIP. It is observed that the variance of coupled O–A contrast is larger than that of ensemble mean AMIP only in the subtropical region. It is also noticed that the highest overestimation of coupled variance by the variance of ensemble mean O–A contrast appears in relatively higher latitudes where the coupled air temperature is not significantly more variable than that of AMIP. This leads us to wonder if the violation of BB98 for the midlatitude air temperature variability is strongly tied to the disagreement in representing thermal interaction between the GCM and the conventional view (BB98).

The correlation coefficients of O–A contrast with SST presented in Fig. 3a for the coupled simulation and in Fig. 3b for the ensemble mean AMIP simulation support our view. Since an efficient positive O–A contrast would warm the SST, positive correlation with SST is expected if O–A contrast causes SST anomalies, while negative correlation with SST is expected if O–A contrast causes damping of SST. The O–A contrast from the ensemble mean AMIP simulation shows strong negative correlation coefficients over all of the North Pacific, confirming that this simulation is driven by SST (Fig. 3b). Meanwhile, the coupled O–A contrast in Fig. 3a exhibits positive correlation coefficients with SST in the subtropics, but insignificant or negative correlation with SST in midlatitudes. This implies that the previous view considering O–A contrast as an external source of SST variability may be valid only in the subtropics.

Instead of O–A contrast, there are indications that wind-induced heat fluxes may dominantly drive the SST variability in midlatitudes. In Fig. 4a, the covariance of the first-layer tendency of heat content (Q_{dTdt}) with SST is shown. As the first-layer tendency indicates, the most prominent positive covariance with SST ap-

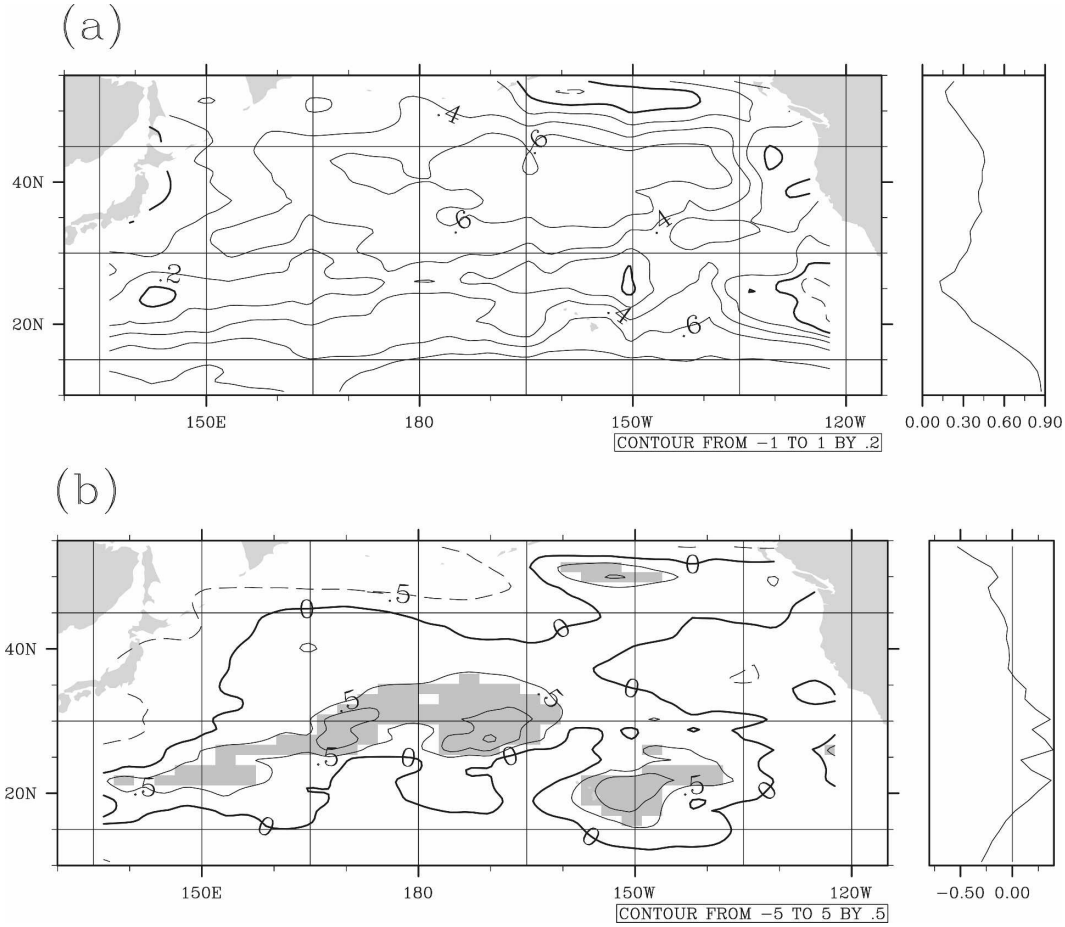

FIG. 2. (a) Correlation coefficients of O–A contrast of temperatures ($H = T_a - T_o$) between ensemble mean AMIP (H^E) and COUP (H^C). Contour interval is 0.2. (b) Deviation of the response-to-coupled variance ratio from one, for O–A contrast [$\sigma^2(H^E)/\sigma^2(H^C) - 1$]. Contour interval is 0.5. Shaded in gray, if the hypothesis for Bretherton and Battisti [2000; H_o: $\sigma^2(H^E)/\sigma^2(H^C) > 1$] is accepted with 95% significance by the f test. Zonal averages are presented on the right.

pears at lag +1 (tendency leads SST) due to the forcing for SST, while the strongest negative covariance with SST appears at lag −1 (SST leads tendency) due to the damping for SST. Furthermore, the lagged covariance exhibits a balanced antisymmetric structure between the negative and positive lags. To see how heat fluxes contribute to the tendency of heat content, the covariance of heat fluxes is additionally presented by components. When the SST leads the heat flux by one month (lag −1), the covariance of turbulent heat flux (Q_{srf}: latent + sensible) with SST recovers 80% of the first-layer tendency. On the contrary, at lag +1, the covariance of turbulent heat flux with SST recovers only one-third as much as that of the first-layer tendency. Furthermore, the covariance with SST shown separately for static adjustment through O–A contrast (Q_θ) exhibits no significant positive covariance at positive lags. By adding the anomalous Ekman advection (Q_{Ek}) to the wind-driven heat flux ($Q_{|U|}$), the covariance wind-induced forcing ($Q_{\text{tot}} = Q_{|U|} + Q_{\text{Ek}}$) with SST becomes two-thirds as high as that of the first-layer tendency (Q_{dTdt}). This clearly shows the dominance of the wind-driven forcing in driving SST. As suggested by the previous studies (Cayan 1992), the heat flux driven by O–A contrast in this region may explain the surface heat flux variability predominantly, but this may not be associated with the driving of SST variability but with the damping of SST variability. The rest of the covariance at lag +1 could possibly be attributed to other oceanic processes, such as anomalous entrainment of cold subsurface water due to the mixed layer fluctuation (Battisti et al. 1995; Dommenget and Latif 2002), radiation heat fluxes associated with cloud variability (Norris et al. 1998), or other ocean dynamics (Czaja 2003). Also, the strong positive covariance between the heat flux and SST can be partly due to the longer at-

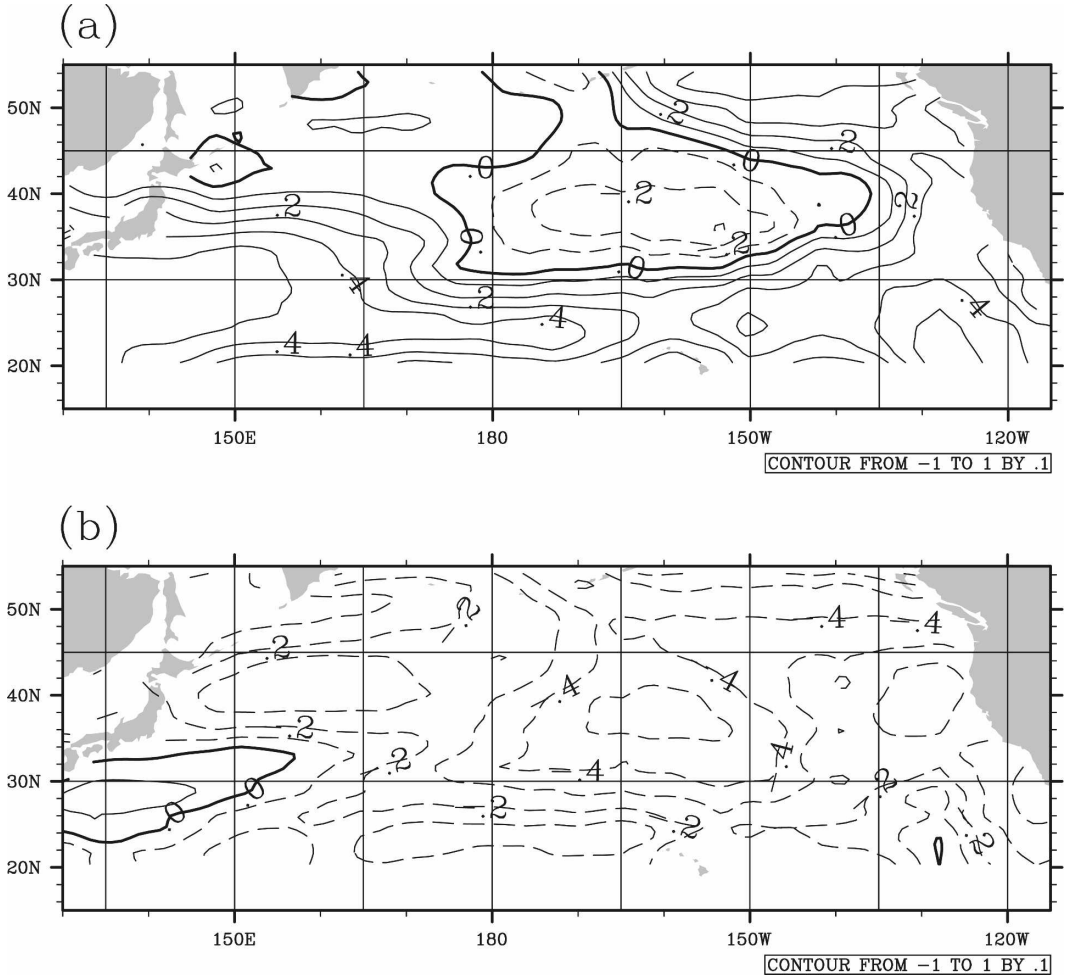

FIG. 3. Correlation coefficients of O–A contrast ($H = T_a - T_o$) with local SST (a) for COUP H^C, and (b) for ensemble mean AMIP H^E.

mospheric persistence associated with the tropical influence (Alexander and Deser 1995; Alexander et al. 2002).

Meanwhile, in the subtropics (Fig. 4b), up to 80% of the covariance of the first-layer tendency with SST is explained by the latent and sensible heat fluxes alone. Ekman advection appears relatively insignificant as forcing for SST in this regions. As shown at negative lags, the latent and sensible heat flux contributes to the damping of SST. The positive covariance of the latent and sensible heat with SST at lag 0 indicates that there is more damping contributed by oceanic processes, such as vertical mixing and lateral advection.

Some caveats contained in Fig. 4 deserve mention here. It is possible that the random noise forcing at higher frequencies is depressed by monthly averaging (Frankignoul et al. 1998), which may exaggerate the damping effect. Also, positive covariance associated with wind-driven forcing partially originated from tropical Pacific through the atmospheric bridge (Frankignoul and Kestenare 2002; Alexander et al. 2002).

4. The role of wind-induced forcing for SST

It is often overlooked that the O–A interaction in BB98 is only through the anomalous O–A contrast of temperature anomalies (Fig. 5a). From this conventional point of view, the SST increases following the warming of surface air, and then air temperature persists longer than its uncoupled persistence, owing to the response to the warm SST. Since SST is perturbed only by static adjustment to lessen the anomalous O–A contrast, the air temperature driven by the prescribed SST is constrained to be less variable than the fully coupled air temperature owing to the missing half of the coupling procedure.

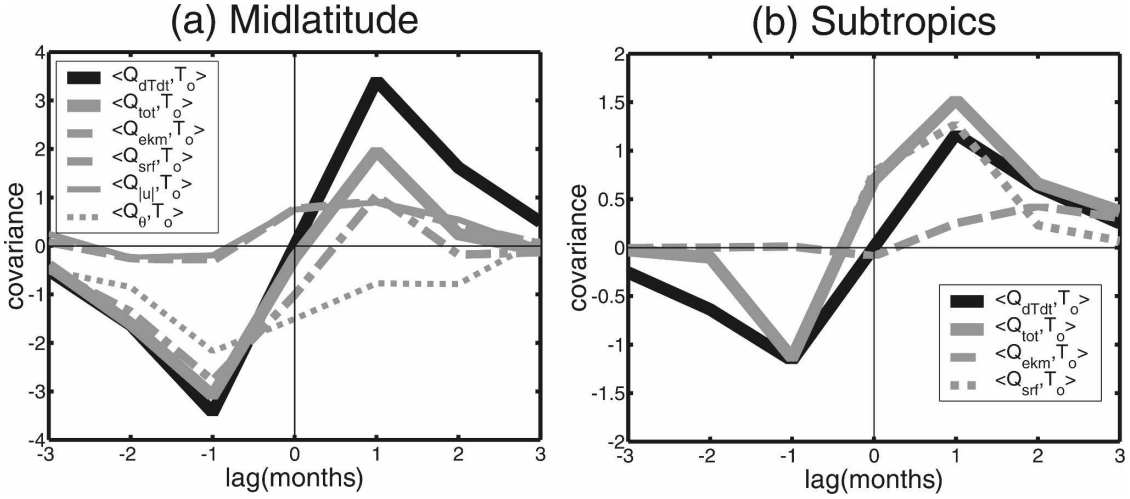

FIG. 4. Covariance of heat fluxes with local SST (T_o) in (a) the midlatitude North Pacific (averaged over 35°–45°N, 180°–230°E) and (b) the subtropical North Pacific (averaged over 20°–30°N, 160°–210°E). Here Q_{dTdt} indicates tendency of the first-layer heat content (layer thickness: 20 m), Q_{tot} indicates the sum of the Ekman advection and the latent and sensible heat fluxes, and Q_{srf} denotes the latent and sensible heat fluxes; $Q_{|U|}$ and Q_θ denote the linearly separated components of latent and sensible heat fluxes, associated with wind speed and O–A contrast, respectively. Ekman advection is only partially considered ($Q_{\text{Ek},z=0} \approx 0.5Q_{\text{Ek}}$). Heat flux is positive downward. Negative lag indicates SST leads.

In contrast to the BB98 speculation, the previous sections exhibit the implications that heat flux due to the adjustment against the O–A contrast represents a damping process for SST, rather than both random forcing and damping in the midlatitude North Pacific. Instead, wind-induced heat flux predominantly forms SST anomalies. Many studies attribute SST variability in midlatitudes to the wind-induced heat flux: wind–

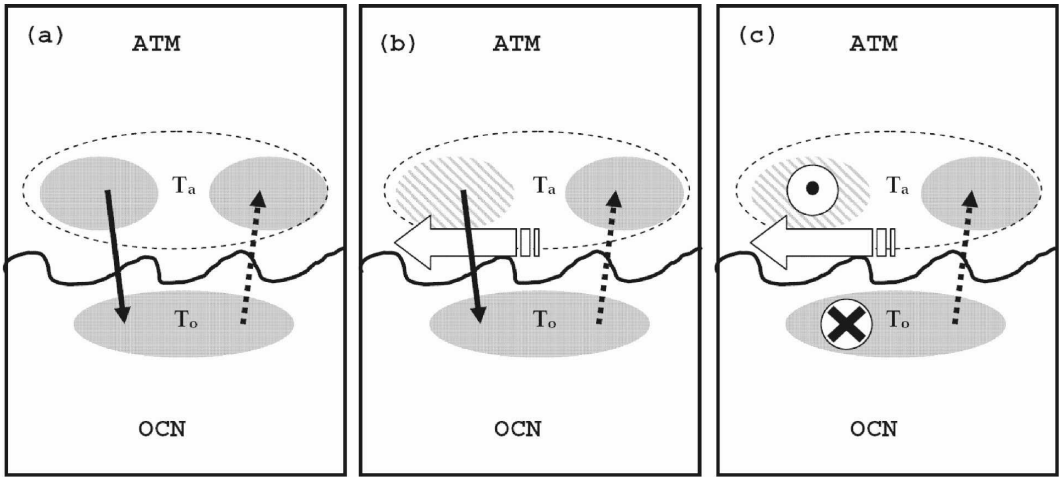

FIG. 5. Illustrations for coupling procedures in the northern midlatitudes. (a) Warm air temperature anomaly (T_a) generates warm SST anomaly (T_o), which causes further warming of the air temperature anomaly, as suggested by BB98. (b) While the reduced wind speed due to an easterly wind anomaly causes a warm anomaly for T_o, it accompanies a cold anomaly for T_a because of heat loss to the ocean. In response to T_o, T_a increases and damps the cold anomaly. (c) While the northward Ekman drift due to an easterly wind anomaly transports warm water for T_o, it accompanies a cold anomaly for T_a because of the atmospheric Ekman transport in the opposite direction. In response to T_o, T_a increases and damps the cold anomaly. Gray shading indicates warming while dashed gray shading indicates cooling. The solid black arrow implies stochastic forcing for SST, while the dashed black arrow denotes the response to the ocean. The white wide arrow is anomalous zonal wind velocity. The white circle with a black dot indicates southward Ekman transport, while the circle with × indicates northward Ekman transport.

evaporation heat flux and temperature perturbation due to wind-driven surface ocean dynamics (Seager et al. 2001; Pierce et al. 2001; Dommenget and Latif 2002; Schneider et al. 2002; Czaja et al. 2003; Lee and Liu 2004; Lee 2006), including the anomalous Ekman advection, on which this study is focused. Indeed, the wind dependence of midlatitude SST variability may not be sufficient enough to report, but leads us to reconsider its impact on the coupled system.

With dominant wind-induced heat flux, the warming of surface air is not a necessary condition to form warm anomalies in SST. Rather, surface air is expected to lose heat as the wind-induced forcing warms SST, and vice versa. In Figs. 5b and 5c, the schematic diagrams depict the impact of both types of wind-induced heat flux on air temperature and SST variability. In midlatitudes, when the wind–evaporation heat flux is the dominant heat flux for SST, it is natural to expect that reduced wind speed causes anomalous cooling for air temperature due to the loss of heat used in forming warm SST anomalies (Fig. 5b). Furthermore, Ekman drift due to the easterly wind anomaly associated with the decreased wind speed in the same region causes further warming in SST by northward advection of the warmer water (Fig. 5c). Due to the strong mean SST gradient, Ekman transport can play a significant role in midlatitudes. In the fully coupled system, Ekman advection would cause further reduction in the air temperature between the response to SST and pure random forcing. If the system is forced by the prescribed SST, no cancellation would occur but only the response to SST would repeat.

How important is the wind-induced heat flux for SST relative to the heat flux for air temperature? The relative magnitude of wind-induced heat flux for SST with respect to the wind-induced heat flux for air temperature essentially depends on the combined effect of both wind-related mechanisms. This can be approximated based on the simple bulk formulas and climatology. For simplicity in this section, the pure random forcing for air temperature in BB98, which was defined as "dynamical forcing" for air temperature, is confined to the wind–evaporation heat flux ($-Q_{|U|}$ positive downward) only. Since this study investigates the effect of wind-induced heat flux in forming anomalies in both SST and air temperature, other irrelevant components for air temperature are set aside for later discussion. This is not to overlook other factors, but to focus on the role of wind-induced heat flux for SST in the coupled system. If we include other types of forcing for air temperature, it would indirectly affect SST through the static adjustment against the O–A contrast, as suggested by the traditional view (BB98). In the next section, a linear model will be developed considering both effects. Also, the nonlinear part of the turbulent heat flux is excluded for simplicity, although its contribution is known to be small but nonnegligible (Lee 2006).

For air temperature, the wind-dependent heat flux $F_{a,U}$ is assumed as

$$F_a = -Q_{|U|}, \tag{4.1}$$

where subscript a indicates an atmospheric term: $Q_{|U|}$ indicates the downward heat flux due to the wind–evaporation effect. Also, the direct wind-induced heat flux for SST, F_o, is considered. In this study, this term is represented by the lateral heat flux associated with anomalous Ekman advection. As speculated in the previous section, as for the wind–evaporation effect, it is reasonable to consider that heat loss in lowering air temperature is gained in increasing SST, and vice versa. Now that the heat flux for the atmosphere is assumed to be purely wind driven, it seems fair to assume the wind-induced heat flux for ocean is also dependent on the same wind synchronously, thereby proportional to the heat flux for atmosphere with a coefficient, ε; that is,

$$F_o = (Q_{|U|} + Q_{\mathrm{Ek}}) = \varepsilon F_a. \tag{4.2}$$

More explicitly, the turbulent heat flux due to the change in wind speed, $Q_{|U|}$, is expressed as a linear form based on the bulk formula (Smith 1988)

$$Q_{|U|} = (L_E \rho_a c_e \overline{q_a - q_o} + c_p \rho_a c_h \overline{T_a - T_o})|u|' = -C_1|u|'. \tag{4.3}$$

Here we focus on only the forcing induced by zonal wind for its dominance over meridional wind in general. Meanwhile, in the ocean, Q^o_{Ek} is given as

$$Q_{\mathrm{Ek}} = \frac{c_o(\rho_a C_D|\overline{u}|)}{f}\frac{\partial \overline{T}_o}{\partial y}u' = -C_2 u'. \tag{4.4}$$

The coefficients C_1 and C_2 are introduced to measure the dependence on the zonal wind perturbation. Descriptions for the symbols used in Eqs. (4.1)–(4.4) are presented in Table 1.

The relative magnitude of wind-induced forcing for SST with respect to that used for air temperature, ε, can be approximated as below, according to Eqs. (4.1)–(4.4):

$$\varepsilon = \frac{\mp C_1 - C_2}{\pm C_1}. \tag{4.5}$$

Under the influence of trade winds in the subtropics and westerly winds in the midlatitudes, it is important to note that positive zonal wind velocity results in reduced wind speed in the subtropics ($Q_{|U|} = C_1 u'$), while

TABLE 1. Typical values used in bulk formulas in calculating wind-induced heat fluxes (wind speed effect and Ekman advection).

Notation	Subtropics	Midlatitudes	Description
$\overline{q_a - q_o}$*	−4	−2	Typical difference of winter-mean surface specific humidity to the mean saturated specific humidity (g kg^{-1}).
$\overline{T_a - T_o}$*	−2.0	−2.5	Typical difference of winter-mean surface air temperature to the mean sea surface temperature (K).
$\overline{(\partial T_a/\partial y)}$*	0.5×10^{-5}	1×10^{-5}	Typical meridional gradient of winter-mean surface air temperature (K m^{-1}).
$\overline{(\partial T_o/\partial y)}$*	0.5×10^{-5}	1×10^{-5}	Typical meridional gradient of winter-mean sea surface temperature (K m^{-1}).
$\lvert\overline{u}\rvert$*	8.5	10.5	Winter mean wind speed at 10-m height (m s^{-1}).
C_D**	0.98×10^{-3}	1.1×10^{-3}	Drag coefficient.
c_h**	0.90×10^{-3}		Sensible heat transfer coefficient.
c_e**	1.35×10^{-3}		Latent heat transfer coefficient.
C_1	18	11	Dependence of turbulent heat flux on wind speed [W m^{-2}(m s^{-1})$^{-1}$].
C_2	1.9	7	Dependence of oceanic Ekman advection on zonal wind velocity [W m^{-2}(m s^{-1})$^{-1}$].
ε	−0.9	−1.4	Relative magnitude of the direct stochastic forcing for ocean to the stochastic forcing for atmosphere (dimensionless).
$\tilde{z}^{-2}$	0.7	1.4	Response-to-coupled variance ratio. The estimated parameters from the observation are used. The wind dependence of air temperature, α, is assumed as 1.
$1 - 2(\tilde{z} - 1)\tilde{z}^{-2}$	0.8	1.4	Expected ratio of AMIP to COUP variance, with wind dependence of air temperature, α assumed as 1.

* da Silva et al. (1994).
** $C_D = (0.44 + 0.063|U|) \times 10^{-3}$, where c_p is specific heat of air, and c_o is specific heat of water (Smith 1988).

it accompanies enhanced wind speed in the midlatitudes ($Q_{|U|} = -C_1 u'$). Therefore, $\varepsilon_{\rm st}$ for subtropics and $\varepsilon_{\rm ml}$ for midlatitudes can be obtained from the relationship below:

$$\varepsilon_{\rm st} = \frac{+C_1 - C_2}{-C_1} \quad \text{and} \quad \varepsilon_{\rm ml} = \frac{-C_1 - C_2}{+C_1},$$

where the coefficients C_1 and C_2 are positive. Considering that atmospheric Ekman advection is small, this relationship implies that it is more likely for ε to be negative.

Typical values for the subtropics and midlatitudes are applied to the actual estimation of ε. In Table 1, all typical values based on the winter mean [December–February (DJF)] climatology are presented, as well as C_1 and C_2. The contribution of atmospheric Ekman drift is omitted since it is negligible compared to that of the wind speed–induced turbulent heat flux, C_1. According to this approximation, it appears that a relatively larger amount of wind-induced heat source is provided for the midlatitude SST than for the air temperature due to the coherent ocean dynamics with the wind-driven heat flux. In midlatitudes, where the mean westerly is dominant, the wind velocity anomaly causes roughly the same wind speed anomaly. The wind–evaporation heat flux and the Ekman advection, combined together, form about 1.4 times larger heat flux in magnitude for SST than that for air temperature. These effects not only provide SST with anomalous heat flux, but also take the same amount away from air temperature; that is, ε is negative.

In the subtropical ocean, the wind-induced forcing for SST is in the opposite direction to that for air temperature, but is only 0.9 times as large as the forcing for air temperature. Ekman advection slightly cancels out the wind speed–induced heat flux, which weakens the wind-induced forcing for SST.

Here, the relative magnitude of wind-induced forcing for SST in the GCM is also roughly approximated using a linear model for heat fluxes. Assuming that the each heat flux component consists of responses to SST and pure random forcing, the heat flux for SST (Q_o), consisting of Ekman advection ($Q_{\rm Ek}$) combined with wind-induced turbulent heat flux ($Q_{|U|}$), can be expressed as

$$F_o = Q_{|U|} + Q_{\rm Ek}.$$

Using monthly mean GCM simulations, the wind-driven turbulent heat flux is approximated based on the multiple linear regression of turbulent heat flux with O–A contrast and wind speed as independent variables. The wind-induced surface turbulent heat flux (latent + sensible) is separated from the following equation for the turbulent heat flux:

$$Q_{\rm srf} \approx Q_{|U|} + Q_\theta = q_{|U|}|U|' + q_\theta(T'_a - T'_o),$$

where the second term indicates the thermal adjustment to the O–A contrast.

The parameter ε based on Eqs. (4.1) and (4.2) is presented as a function of location (Fig. 6). Overall, as speculated with observed climatology in this section, it is implied that more negative ratios are located in midlatitudes, while less negative ratios are located in the

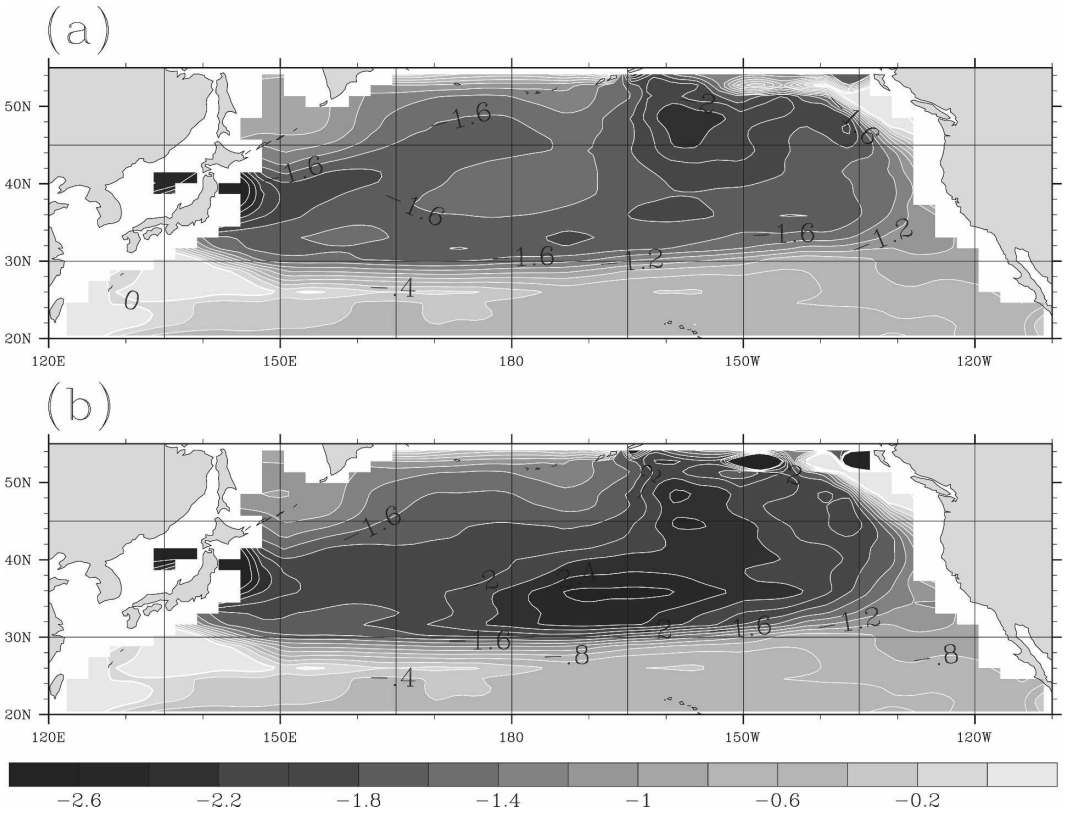

FIG. 6. The wind-induced forcing parameter ε for SST (a) with the tropical influence filtered by the linear regression against the model Niño-3.4 index and (b) with the tropical influence included. The coupled GCM results are used. See the main text for detailed estimation.

subtropics. However, the approximation may contain uncertainties, partly owing to atmospheric persistence associated with remote tropical influence. Without the influence from tropical Pacific, it is observed that the wind-induced forcing for SST is about 1.5 times as strong as that for air temperature in midlatitudes, while it is only 0.6 times as strong as that for air temperature in the subtropics (Fig. 6a). Compared to the calculation without filtering the signal from tropical Pacific (Fig. 6b), the parameter ε is reduced most in the central midlatitude Pacific by filtering the tropical influence, while no significant change is found in the subtropics. The error in the linear separation of the surface heat flux could be another major source of uncertainty. Special caution is advised for using subtropical values since the mean wind speed is substantially underestimated owing to monthly averages.

5. Extending BB98 to the wind-induced SST

a. The response to coupled variance ratio

A new linear coupled model is suggested as an extension of BB98, with wind-induced heat flux for SST. Actually, the wind-induced heat flux for SST has been suggested by previous studies (Liu 1993; Saravanan and McWilliams 1998), but neglected for simplicity. The theoretical stance taken here is not far from the basic ideas by BB98. It is still agreed that the major source for extratropical SST variability is provided by the atmospheric internal variability. The coupled system is still considered in a vertical column. In addition to BB98, first of all, more realistic heat fluxes are considered. As illustrated earlier in this paper, wind-induced surface heat flux explicitly serves as the forcing both for air temperature and SST. Second, ocean dynamics is considered. Only the simplest dynamics, Ekman advection due to anomalous wind stresses, is included as the additional wind-induced forcing for SST. Although this may oversimplify the full ocean GCM, following the framework of BB98 would still be efficient enough to explore the broadband characteristics of the interannual or longer time scale coupled variability. In the similar response time, the wind stresses can also contribute to the SST anomalies by perturbing the mixed layer thickness. As pointed out by previous studies (Battisti et al. 1995; Dommenget and Latif 2002),

anomalously stronger wind stresses may cause excessive cooling of the sea surface by the anomalous entrainment of colder subsurface water. Mainly due to wind speed, this effect may intensify the wind-driven surface heat flux for SST both in the midlatitudes and subtropics. Although not explicitly mentioned here, it must be taken into account that the wind-driven heat flux for SST is partly attributed to the variation of the mixed layer thickness due to anomalous vertical mixing.

In this study, the coupled linear model is forced by two types of heat fluxes. The heat flux for air temperature (F_a) is determined according to physical causes. Here, the forcing includes both static (F_θ) and dynamic (F_U) components ($F_a = F_\theta + F_U$). The static heat flux F_θ indicates the component associated with the vertical gradient of air temperature or humidity. Following the design by BB98, static forcing indirectly affects SST through coupling with air temperature. In addition to static heat flux, dynamic heat flux F_U is included. Independent of static heat flux, dynamic heat flux directly affects both air temperature and SST. As illustrated earlier, it is highly likely that winds perturb air temperature and SST in opposite directions by the flux transport of anomalous heat from one to another ($\varepsilon < 0$). It is worth mentioning that it is also possible for the direct heat flux to affect both SST and air temperature in the same direction owing to nonlinear heat fluxes if the dynamic and the static components are somewhat coherent or, similarly, if multiplicative noise-type heat flux is important (Sura et al. 2006). This case is not fully considered here, but can be implicitly represented by the case of a positive wind-induced forcing parameter, $\varepsilon > 0$. Now, the extended linear coupled model is defined as below:

$$\gamma_a \frac{dT_a}{dt} = -\lambda_{sa}(cT_a - T_o) - \lambda_a T_a + F_\theta + F_U$$

$$\gamma_o \frac{dT_o}{dt} = \lambda_{so}(cT_a - T_o) - \lambda_o T_o + \varepsilon F_U, \qquad \text{(extended BB98)}$$

where subscripts o and a refer to ocean and atmosphere, γ represents the heat capacity of each medium, λ_s indicates the dependence of turbulent heat fluxes on O–A temperatures difference, λ is the intrinsic damping rate in each medium, and c is the calibration factor for air temperature at the surface. The heat flux F consists of the dynamic response to SST and pure random forcing, N [$F = (b - 1)T_o + N$]. The pure random forcing consists of static and dynamical components, which are assumed independent for simplicity. The subscripts θ and U indicate static forcing and dynamical forcing, respectively. The dependence on dynamical forcing is denoted as α and the dependence on static forcing is set as $\sqrt{1 - \alpha^2}$. Then, the equations are transformed into frequency domain:

$$(i\sigma + a)T_a^C = bT_o + \sqrt{1 - \alpha^2}N_\theta^C + \alpha N_U^C$$

$$(i\beta\sigma + d')T_o = cT_a^C + \varepsilon\alpha N_U^C \qquad (5.1)$$

for COUP

$$(i\sigma + a)T_a^M = bT_o + \sqrt{1 - \alpha^2}N_\theta^M + \alpha N_\theta^M \qquad (5.2)$$

for AMIP

$$(i\sigma + a)T_a^E = bT_o \qquad (5.3)$$

for ensemble mean AMIP. The superscript M denotes AMIP-type simulation in which SST (T_o) is prescribed, E refers to the infinite ensemble mean of AMIP-type simulation, whereas C indicates full coupling. Since the ensemble mean of AMIP simulation depends only on SST, this can be called the response to SST. The estimated parameters based on our GCM simulations are provided in Table 2. The formulation of positive parameters a, b, c, and d follows that of BB98. Also, σ indicates unit frequency ($\sigma = \gamma_a\omega/\lambda_{sa}$), where the ratio of heat capacity is defined as $\beta = \gamma_o\lambda_{sa}/\gamma_a\lambda_{so}$. The oceanic damping parameter d' is now defined as $d' = d + \varepsilon(1 - b)$. While being transformed, the heat exchange coefficients used in the ocean and the atmosphere are assumed to be the same since there is only a negligible difference in the original equations (BB98: $\lambda_{sa} \approx \lambda_{so}$). Following BB98, dynamical response parameter b is designed to reduce or enhance the background damping of SST ($b = 1$). However, in the extended model, parameter b can indicate opposite dynamical responses, depending on the dominant heat flux for SST. Assuming $\alpha = 1$ for simplicity, in the case of a negative response, response to SST and the random forcing are in opposite directions; that is,

$$(b - 1)T_o N^C < 0.$$

TABLE 2. Estimated parameters for the extended linear model. For the GCM of the North Pacific, the temperatures of the midlatitudes are averaged from 34° to 45°N, 130°W to 180° and for the subtropics from 20° to 30°N, 150°W to 160°E. For observations, temperatures are gathered from ICOADS 2° × 2° enhanced dataset (http://icoads.noaa.gov/), for the period 1969–99.

	GCM		Observations	
	Midlatitudes	Subtropics	Midlatitudes	Subtropics
b/a	0.81	0.88	1.00	0.68
c^*	0.29	0.46	0.58	0.37
d^*	0.37	0.86	0.73	0.62
$\hat{z}(=\lvert ad'/bc\rvert)$	1.57	2.17	1.26	2.48

Using Eq. (5.1), this can be rewritten as

$$\frac{(a\varepsilon + c)(b-1)}{ad' - bc}|N^C| < 0.$$

It is implied that the dynamical response parameter larger than 1 ($b > 1$) and the dominant wind-induced heat flux for SST ($\varepsilon < -c/a$) form negative dynamical response to SST, while the dynamical response parameter less than 1 and the dominant static heat flux for SST ($\varepsilon > -c/a$) form the same.

With the parameter for wind-induced heat flux for SST, the new stability condition is established in order to result in a competition between the damping and forcing as in BB98:

$$\hat{z} = \frac{ad'}{bc} = \frac{a[d + \varepsilon(1-b)]}{bc} > 1.$$

The coupled solutions are stable when $\hat{z}$ is greater than 1. Now, the stability condition provides upper and lower bounds of the wind-induced heat flux for SST (ε) depending on the dynamical feedback (b):

$$\begin{cases} \varepsilon < \dfrac{bc - ad}{a(1-b)}, & b > 1 \\ \varepsilon > \dfrac{bc - ad}{a(1-b)}, & b < 1. \end{cases}$$

These constraints simply imply that, in the case of a positive dynamic feedback that is too strong, the solution becomes unstable.

Under the low-frequency assumption ($\sigma \to 0$), the ratio of response to coupled variance, interpreted practically as the potential predictability, can be derived as

$$\tilde{z}^{-2} = \frac{\sigma^2(T_a^E)}{\sigma^2(T_a^C)} = \frac{(bc + ab\varepsilon)^2 + b^2c^2(1-\alpha^2)\alpha^{-2}}{(ad' + ab\varepsilon)^2 + a^2d'^2(1-\alpha^2)\alpha^{-2}}, \quad (5.4)$$

where $d' = d + \varepsilon(1-b)$. It is important to note that the response variance can exceed the coupled variance; that is, $\tilde{z}^{-2}$can be larger than one by including the wind-induced heat flux for SST. It can be shown that $\tilde{z}^{-2}$ approaches to z^{-2} of BB98 with $\varepsilon \to 0$ and $\alpha \to 0$. In BB98, the response-to-coupled variance ratio is equivalent to the stability parameter ($\hat{z}$ with $\alpha = 0$ and $\varepsilon = 0$). In this case, the response variance is restrained from outgrowing the coupled variance for the sake of stability. However, with efficient wind-induced heat flux for SST (T_o), the response variance can exceed the coupled variance ($\tilde{z}^{-2} > 1$) without compromising stability.

Additionally, the variance due to two-way interaction out of the coupled variance is derived as

$$\frac{\sigma^2(T_a^C) - \sigma^2(T_a^M)}{\sigma^2(T_a^C)} = 2(\tilde{z} - 1)\tilde{z}^{-2}. \quad (5.5)$$

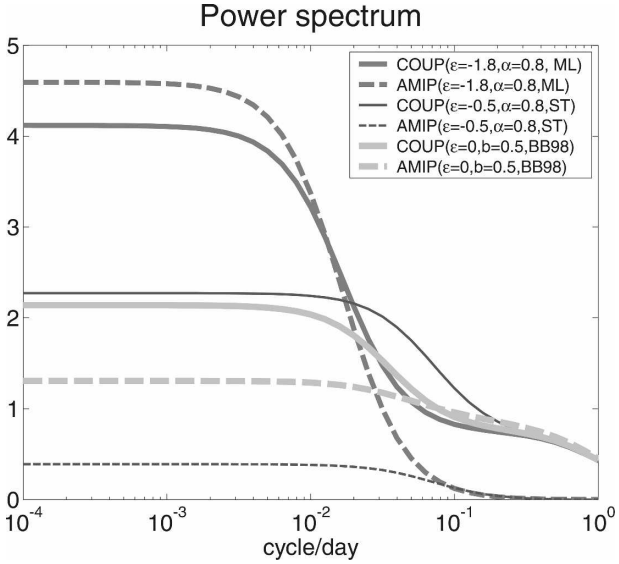

FIG. 7. The analytical power spectra for the surface air temperature. The parameters for the linear coupled model are the estimated values based on the air temperature (T_a) and SST (T_o) of the GCM results (see Table 2).

Another important implication emerges here. Wherever the response variance is stronger than coupled variance ($\tilde{z}^{-2} > 1$), it is also true for the total AMIP variance to exceed the COUP variance, unless there is no response to SST at all. At the bottom of Table 1, the expected response-to-coupled variance ratio, as well as the AMIP-to-COUP variance ratio, is presented according to Eqs. (5.4) and (5.5). For the parameters a, b, c, d', and ε of the linear model, the estimated values based on observation (Table 2) are used. Assuming that the system is purely wind driven ($\alpha = 1$), it is shown that the response variance can be 1.39 times as high as the coupled variance. Also, the AMIP variance becomes 1.42 times as high as the coupled variance. On the other hand, the response variance and AMIP variance are only about 70% of the coupled variance.

Figure 7 presents the repeat of BB98's well-known power spectra. With the previously known theoretical curves, two cases for the subtropical and midlatitude North Pacific are additionally presented. For GCM results, the estimated parameters given in Table 2 are used. The detailed estimation of the parameters for the GCM and its observation is described in the appendix. The parameters for the GCM results are estimated in two North Pacific regions. The stability parameters are less than BB98's estimation at both of locations. The relative magnitudes of wind-induced heat flux for SST (ε) are chosen based on the approximation for the GCM presented in section 3. The wind dependence of air temperature (α) is assumed as 0.8 ($\alpha^2 \approx 0.65$). By

introducing wind-induced heat flux for SST, it is shown at all frequencies that coupled variance can be surpassed by AMIP variance in the midlatitude North Pacific. However, with insufficient wind-induced heat flux for SST as in the subtropics, the response variance would not exceed the COUP variance. Although the AMIP-to-COUP variance ratio is close to one in this case, this is not an indication of perfect simulation by prescribing SST. This would rather be a comparison of the variances of the pure random forcing in both simulations since there is only weak SST variance expected around the subtropics.

To see to what extent and under what circumstances the response variance exceeds the coupled variance, we explore the theoretical ratio by varying the newly defined parameters slightly around the estimated values. The examined parameters are wind dependence of air temperature α, dynamic response to SST b, as well as the parameter for wind-induced heat flux for SST ε. With other parameters set as the estimated values of the midlatitude North Pacific of the GCM (Table 2), and for the low-frequency variability ($\sigma \to 0$), the theoretically driven response-to-coupled variance ratios are presented in Fig. 8.

In Fig. 8a, the ratio is presented as a function of the wind dependence of air temperature ($0 < \alpha < 1$) and its relative contribution to SST ($-5 < \varepsilon < 5$). For the dynamic response parameter b, the approximated value in midlatitudes, is used. To calculate the ratio the atmospheric heat capacity is assumed to be 0.05 times as large as the ocean heat capacity, as suggested by BB98. The more dominantly the wind-induced forcing perturbs the air temperature ($\alpha \to 1$), the more easily the response variance exceeds the coupled variance, if there is exchange of heat by wind-induced forcing with sufficient magnitude ($\varepsilon < -c/a$). The response variance exceeds the coupled variance most predominantly when ε approaches $-d'$ and α to 1. This indicates the extreme coupling in which perfect cancellation occurs between the response to SST and the wind-induced forcing for air temperature. If the wind-induced forcing even more strongly affects SST ($\varepsilon \ll -c/a$), the coupled system becomes ocean driven, which would result in the coupled air temperature explained predominantly by the response to SST. Meanwhile, response variance would not reach the coupled variance, regardless of direct wind-induced forcing, if the wind dependence of air temperature is too weak ($\alpha^2 \to 0$). As shown in Fig. 8a, within a realistic range of the wind-induced forcing for SST, the response variance never exceeds the coupled variance if the wind dependence of air temperature is ignored ($\alpha^2 < 0.1$). According to the study by Alexander and Scott (1997), using uncoupled GCM

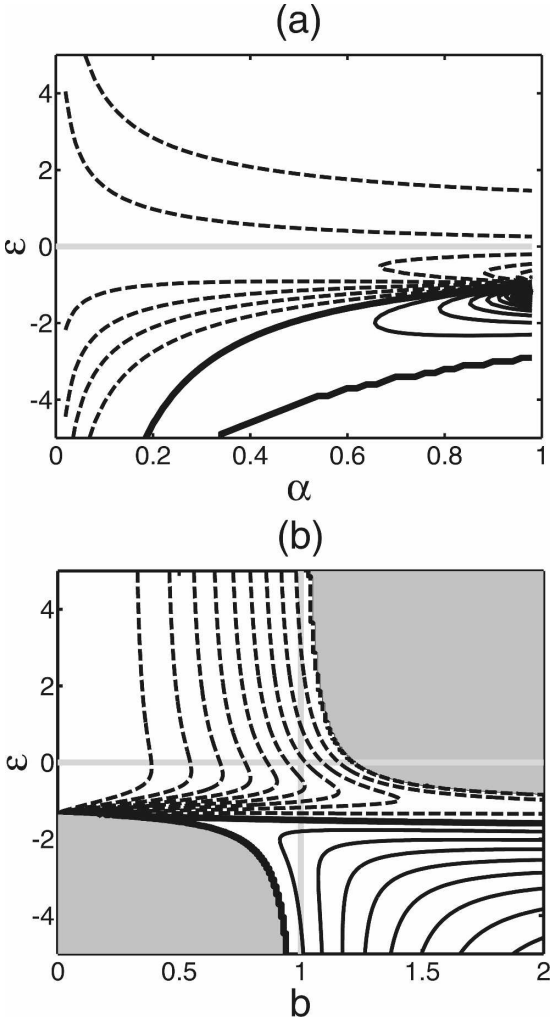

FIG. 8. The analytical deviation of response-to-coupled variance ratio from 1, for the surface air temperature [$\tilde{z}^{-2} - 1 = \sigma^2(T_a^E)/\sigma^2(T_a^C) - 1$]. The parameters for the linear coupled model (see Table 2 for the case of midlatitude GCM) were estimated based on the midlatitude North Pacific air temperature (T_a) and SST (T_o) of the GCM results. (a) With respect to the wind dependence (α) of air temperature [$\alpha^2/\sqrt{1-\alpha^2} = \sigma^2(\eta_{a,U})/\sigma^2(\eta_{a,\theta})$] and the relative magnitude of the forcing for SST ($\varepsilon = F_{o,U}/F_{a,U}$). Dynamical response parameter is set as estimated. (b) With respect to the dynamic response parameter, b and forcing for SST, ε. The wind dependence of atmospheric forcing α is assumed as 0.8 ($\alpha^2 \approx 0.65$). Gray shading indicates the unstable conditions. The dashed and solid lines represent negative and positive values, respectively. Zeroes are contoured in thicker lines. Contour interval is 0.1.

simulations, in the turbulent heat flux the wind dependence of air temperature is stronger in the western half of the midlatitude North Pacific, while the static dependence is stronger in the eastern midlatitude North Pacific.

In Fig. 8b, the theoretical response-to-coupled variance ratio within the a realistic parameter regime of the dynamical response b are presented with respect to the wind-induced forcing for SST, ε. The regions where the

stability condition is violated are shaded gray. The wind dependence of air temperature is assumed comparable with the dependence on static forcing (N_θ); that is, $\alpha^2 = 0.65$. This is based on the study by Alexander and Scott (1997). Using the uncoupled GCM, Alexander and Scott showed that in the midlatitude North Pacific wind-induced heat flux dominates the western half while the static heat flux dominates the eastern half with comparable strength. With no wind-induced forcing for SST ($\varepsilon = 0$), the response variance is less than the coupled variance regardless of the dynamic response, as in BB98. With stronger wind-induced forcing ($\varepsilon \ll 0$), response variance is expected to exceed the coupled variance. Meanwhile, the extremely low ratio emerging around $\varepsilon \sim -c/a$ indicates the minimum SST variability, in which the wind-driven SST remarkably cancels out the opposite effect through O–A contrast. In this case, the response-to-coupled variance ratio converges to zero because the SST anomaly is too weak for air temperature to respond. The AMIP-to-COUP ratio would approach one in this case (not shown) since the strength of internal variability in both systems is assumed to be equal. It is worth mentioning that the response variance exceeds the coupled variance only if the wind-induced forcing for SST acts against the wind-driven forcing for air temperature with sufficient strength; that is, $\varepsilon < -d$. Negative dynamical response lessens the ratio below one and enhances the ratio beyond one, as shown in the upper left and the lower right corners. With stronger negative dynamical response to SST [$\varepsilon(b - 1) < 0$], the response variance would further exceed the coupled variance than it would without a negative dynamical response, if the wind-driven effect is the dominant forcing for SST ($\varepsilon < -c/a$). On the other hand, the response variance would underestimate further the coupled variance, where the O–A contrast effect is dominant in driving SST.

This can be understood quite intuitively. Compared to the case without dynamical response, the stronger the atmospheric dynamics respond negatively to SST, the stronger the damping of SST anomaly would occur, in the case of dominant wind-induced heat flux for SST ($\varepsilon < -c/a$). This intensified response to SST forms more cancellation between the random forcing for air temperature in the coupled simulation. Meanwhile, air temperature becomes more variable in the AMIP simulations without such association between the response to SST and the random forcing. Therefore, the ratio of response-to-coupled variance increases with stronger negative dynamical response, for the numerator increases while the denominator decreases. On the other hand, with the dominant static heat flux for SST ($\varepsilon > 0$), the stronger negative dynamical response to SST weakens the dependence of air temperature on SST. The coupled air temperature would become more variable with a stronger response to SST since the response reinforces the forcing. However, only the reduced dependence on SST would remain in the AMIP air temperature without such association between the response to SST and the random forcing. Thus, the response-to-coupled variance ratio decreases with the stronger negative dynamical response in this case.

b. Ocean–atmosphere interaction

If SST is dominated by direct wind-induced heat flux rather than by static adjustment against the O–A contrast, the air temperature could passively respond to the SST, even under the fully coupled condition. Previously, Bretherton and Battisti 2000 suggested that heat flux in AMIP simulation is erroneous both in strength and direction. In the framework of the BB98 model, the covariance of O–A contrast (H^C) and the response O–A contrast (H^E, ensemble mean AMIP) with SST are expressed at low frequencies ($\sigma \to 0$) as

$$\langle H^C, T_o \rangle = \sigma^2(T_o)(d - 1)$$

$$\langle H^E, T_o \rangle = \sigma^2(T_o)\left(\frac{bc}{a} - 1\right),$$

where the heat fluxes are defined as $H^C = cT_a^C - T_o$ and $H^E = cT_a^E - T_o$. Since $d > 1 > bc/a$ in BB98, the dependence of coupled O–A contrast must be positive and small, while that of ensemble mean AMIP must be negative and excessively strong. This is because BB98 assumed that SST is indirectly affected by random forcing through O–A contrast. With the SST driven by the static adjustment, coupled O–A contrast contains both the forcing for SST and the response to it, while AMIP simulation can repeat only the response to SST. This could be the major cause of the negative correlation coefficients between the O–A contrasts of AMIP and COUP.

However, with the wind-induced heat flux for SST, the covariance of the heat fluxes with SST can be expressed as

$$\langle H^C, T_o \rangle = \sigma^2(T_o)\left(\frac{bc}{a} - 1\right) + \left(\frac{1}{ad' - bc}\right)\left(\frac{c(\alpha^2 a\varepsilon + c)}{a}\right)$$

$$\langle H^E, T_o \rangle = \sigma^2(T_o)\left(\frac{bc}{a} - 1\right).$$

TABLE 3. The covariance between the O–A contrasts of COUP (H^C) and ensemble mean AMIP (H^E) for the GCM North Pacific. Correlation coefficients are presented within parentheses.

	Midlatitudes	Subtropics
$\langle T_o, H^C \rangle$	−0.05 (−0.22)	0.01 (0.10)
$\langle T_o, H^E \rangle$	−0.08 (−0.51)	−0.02 (−0.38)

In these relationships, the COUP O–A contrast can synchronize with SST in the opposite direction as AMIP O–A contrast. This suggests that O–A contrasts represent the damping process for SST in both simulations. Furthermore, coupled O–A contrast is capable of covarying with SST even more negatively than AMIP O–A contrast, where the wind dependence of air temperature is strong and the wind-induced heat flux is dominant in driving SST ($\varepsilon\alpha^2 < -c/a$). This implies that the coupled O–A contrast can be affected by SST more intensively than AMIP O–A contrast. As mentioned in section 3, GCM results indicate that coupled O–A contrast in the North Pacific correlates with ensemble mean AMIP O–A contrast most strongly and positively in midlatitudes, while it does not significantly correlate, or correlates negatively, with ensemble mean AMIP O–A contrast in the subtropics (Fig. 3a). The actual covariance values for both cases are estimated using the area average of O–A contrast and SST in the subtropical and the midlatitude North Pacific and shown in Table 3. It is notable that the covariance and correlation coefficient are negative for both COUP and AMIP O–A contrast with SST in the midlatitude North Pacific, while they are negative only for AMIP O–A contrast with SST in the subtropical North Pacific. These suggest that, in the presence of efficient wind-induced forcing for ocean, the major role of O–A contrast can be damping for SST in both COUP and AMIP. Moreover, with strong wind dependence of both air temperature and SST, "enhanced thermal damping" due to coupling is possible in contrast to the conventional model (BB98).

6. Summary and discussion

A set of GCM experiments indicates that the coupled climate variability may not grow out of AMIP-type simulations in the extratropics. This result is obtained more credibility than the previous GCM studies since the model deficiency is minimized by prescribing the GCM-generated SST for hindcasts. The O–A contrasts simulated by the COUP and AMIP approaches show strong positive correlation coefficients in midlatitudes. Further analyses strongly suggest that the disagreement found in this study and BB98's expectation may be explained by taking into account the wind-induced effects on SST. Covariance analyses of SST and heat flux by components demonstrate that the SST in midlatitudes is predominantly driven by wind-induced forcing, whereas the SST in the subtropics is still under the stronger influence by O–A contrast.

The extended coupled model suggests that the disagreement of GCM results with BB98 can be explained by the disagreement of the coupling mechanism between the two systems. Wind-induced forcing is introduced as the direct forcing for SST, as an extension of BB98. In contrast to the conventional view, the analytically driven response-to-coupled variance ratio shows both overestimation and underestimation of coupled variance by the response variance, without violating the stability constraint. It is mathematically proved that AMIP variance exceeds coupled variance as response variance surpasses coupled variance. The direct wind-induced forcing for SST plays the most important role in determining whether the response variance would exceed the coupled variance. First, the wind-induced forcing must play an opposing role in causing temperature variability between atmosphere and SST. Second, in driving SST variability, the direct wind-induced forcing must be stronger than the indirect forcing through O–A contrast. Wind dependence of air temperature is another important factor. Air temperature must be somewhat dependent on the wind-induced surface heat flux to have a response variance greater than the coupled variance. Also, a negative dynamical response to SST can further enhance the response variance to surpass the coupled variance within the stability constraint. Based on the extended linear model, it is also analytically shown that the O–A contrast of AMIP simulation can be in the same direction as that of COUP, where the coupled system depends on efficient wind-induced forcing for SST. In addition, it is also possible for the variance of the AMIP O–A contrast to underestimate that of COUP if the wind-induced forcing for SST is dominant and the wind dependence of air temperature is not negligible.

It has to be considered as a caveat of this study that the experimental design was set up without excluding the remote influence of the tropical Pacific. However, there are a couple of positive clues to support the credibility of this study. First, the remote influence on extratropical dynamics, such as a Pacific–North America (PNA) like structure, has been reported to be insensitive to local coupling to ocean (Bladé 1999). This might suggest that the intensification in dynamical variability due to prescribing SST is likely to be associated with the local coupling procedure rather than the atmospheric

bridge (Alexander et al. 2002). Second, the violation of BB98 intensifies when the tropical influence is statistically filtered out of our GCM simulation (not shown). For the best understanding on dynamical variability in the extratropics, it would be essential to conduct a set of AMIP-type experiments for the extratropics, while the tropical SST is kept at the mean annual cycle.

In regard to the possibility of a deterministic external forcing, such as remote tropical influence (Alexander et al. 2002), a similar conclusion to this study is expected. The essence of the extended simple model is the ability for the wind-induced forcing to directly force the SST. When two-way interaction is allowed, whether the forcing is deterministic or not, the low-frequency wind-driven forcing synchronously exerts the opposite effect on air temperature while it forces the SST. With no dynamical response, it could be easily tested using the linear model forced by a deterministic forcing if the analytical response-to-coupled variance ratio is well reproduced.

The uncertainty in the estimated dynamical response parameter may alter quantitatively the conclusion of this study, but would not essentially contradict it, as far as the system is kept stable. The stronger the negative dynamical response to SST is, the more easily the response variance underestimates the coupled variance in the conventional, statically driven system. On the contrary, in a dynamically driven system, the stronger the negative dynamical response to SST is, the more the response variance exceeds the coupled variance. Due to the tropical influence through the atmospheric bridge (Alexander et al. 2002), the dynamical response parameter b is expected to misrepresent slightly the extratropical coupling. If the persistence due to external causes could be completely excluded, the actual parameter would be either more negative or less positive. Our analytical speculation indicates the further overestimation of coupled variance by response variance in the midlatitude North Pacific without the tropical influence. Also, if there was an additional "warm low"–type negative dynamical response in the extratropical Pacific, as suggested by various modeling studies (Sutton and Mathieu 2002; Yulaeva et al. 2001; Liu and Wu 2004), it would be more likely for AMIP to overestimate the coupled variance in the midlatitude North Pacific. Meanwhile, with additional positive dynamical response to SST (Peng and Whitaker 2000), it would be less likely for the same to occur.

The recurrent forcing due to a local dynamical response to ocean has to be further explored. It has been found that the variance of AMIP sea level pressure exceeds substantially the coupled variance at any location in the North Pacific (not shown). Statistically, the overestimation of COUP variance by AMIP variance may indicate there is negative covariance between the response and forcing when fully coupled. Assuming that there is no impact other than local O–A interaction, this can be understood as the negative dynamical response. It is tempting to conclude that this negative dynamical response also can be attributed to the wind-induced SST in midlatitudes, similar to the case for air temperature. But this would remain unclear until the pure local O–A interaction is examined using GCM experiments without remote influences.

This study takes a stance following the atmosphere-centric viewpoints, which considers the ocean as a passive heat capacitor without the capability of selecting the time scale (Frankignoul and Hasselman 1977; BB98; Saravanan and McWilliams 1998). With the least complexity for the ocean, however, it is clearly shown that the role of the ocean in the extratropical climate variability is essential enough to reject the previous expectation on the coupled climate variability. As the previous modeling study speculated (Pierce et al. 2001), considering the relatively short response time and the intensity, Ekman advection is the most feasible candidate to explain the background red noise without specific preference on time scale. Ekman advection plays in concert with wind-induced surface heat flux to gain dominance over the static forcing in driving the SST in the midlatitudes.

Yet, the gap between GCM simulations and the BB98 model found in this study cannot be thoroughly explained by red noise–type wind-induced SST. There are somewhat important terms neglected for simplicity. First, the variation of the mixed layer thickness is closely related to the nonlinear processes, which are not fully examined in this study. Deepening of mixed layer depth can contribute to both enhancement and reduction of the SST variance by lengthening of persistence and dilution of forcing, respectively. Second, entrainment of subsurface water due to wind forcing can cause SST anomalies (Battisti et al. 1995; Dommenget and Latif 2002). The reemergence of anomalous subsurface temperature also enhances the strength of coupling by maintaining the year-to-year persistence (Alexander et al. 2002). Third, thermocline wave dynamics and oceanic gyre circulation can be dominant in the regions of active dynamics, especially at low frequencies. For example, in western boundary regions or the regions of active thermohaline circulation, SST is far from red noise (Hall and Manabe 1997). As Czaja (2003) suggested, anomalous Ekman advection may be a dominant forcing for SST only at relatively higher frequencies ($\lesssim$0.5 cycles per year) in midlatitudes. Ocean dynamics may cause frequency-dependent SST variability, which is included in GCM simulation but neglected

in the context of a linear stochastic model. Also, the continuously varying sensitivity of atmosphere to SST could remarkably affect the SST (Sura et al. 2006). There is no doubt about the necessity for an intermediate model with various dynamical oceanic processes. By projecting the one-dimensional temperature model onto the basin-scale dynamics, we could only partially explain the coupling with red noise–type SST variability. To step forward, frequency-dependent phenomena must be explored using a simple model with more complexity in ocean dynamics. If more complicated oceanic processes such as Rossby wave dynamics were taken into account, more frequency-dependent behaviors would be expected (S.-I. Shin 2007, personal communication). Since our GCM includes full ocean dynamics, the impact of more complex ocean dynamics could also be investigated. To explore low-frequency phenomena more closely, studies on the expansion of the GCM experiments both in length and number would be required in the future.

A practical remark from this new aspect of midlatitude O–A interaction is that, aside from the fundamental question of predictability in extratropics, the response-to-total ratio can be fictitiously underestimated in midlatitudes, which is often used to measure the potential predictability of the real climate (Harzallah and Sadourny 1995; Rowell 1998; Kang et al. 2004).

Acknowledgments. We thank two anonymous reviewers and the editors for their valuable comments and suggestions. Lee thanks Sang-Ik Shin at CDC for the profound discussion. This paper has been funded with assistance from NASA JPL Grant 1228147, with further support from the NSF and NOAA Center for Climatic Research.

APPENDIX

Parameter Estimates in the Coupled GCM

In order for a proper interpretation on the coupled GCM results, one must estimate the parameters using the coupled GCM results. Among several ways to explore the parameter domain, we examine the linear relationships between the air temperature and SST on a monthly time scale (Frankignoul et al. 1998; Czaja et al. 2003). Monthly average substantially reduces the temporal variability of the actual air temperature anomaly, whereas it conserves most of its SSTs. Using monthly means conveniently reduces uncertainty in the parameter estimation due to the persistence of the forcing itself, which could be about a week or two. Based on a first-order Taylor expansion of the linear inverse model (Penland and Sardeshmukh 1995; Penland and Matrosova 1998; Winkler et al. 2001), the coupled equations are discretized as below:

$$0 = aT_a^{i+1} - bT_o^{i+1} + R_a^{i+1} \tag{A.1}$$

$$T_o^{i+1} = c^*T_a^i + (1 - d^*)T_o^i + R_o^{i+1/2} \tag{A.2}$$

where i indicates month, Δt is one month in seconds and

$$c^* = \frac{\lambda_{so}\Delta t}{\gamma_o}\, c,\ d^* = \frac{\lambda_{so}\Delta t}{\gamma_o}\, d';$$

R_a and R_o indicate the residuals.

The parameters were estimated using GCM results, as well as the observation International Comprehensive Ocean–Atmosphere Data Set (ICOADS; $2^\circ \times 2^\circ$ enhanced, 1961–2005) for comparison. Only winter months (October–March) were used. In Eq. (A.1), the tendency of air temperature is omitted since the monthly average is almost dissociated with memory of the previous month. The ratio of the parameter $b : a$ can be estimated using lagged covariance, where negative lags indicate the ocean leading the atmosphere,

$$\langle T_a(0), T_o(-\tau)\rangle = \frac{b}{a}\langle T_o(0), T_o(-\tau)\rangle,$$

where $\tau > 0$ and angle brackets indicate covariance. For observation, covariance at lags -1 and -2 were used. For GCM, AMIP air temperature and the SST were used at lags 0 and -1 since the random forcing in AMIP does not correlate with SST. Meanwhile, Eq. (A.2) exhibits the finite differential form of the continuous SST (T_o) equation with a monthly time step. Using covariance at different monthly lags, the parameters c^* and d^* can be estimated:

$$\begin{cases} \langle T_o(0), T_a(-\tau)\rangle = c^*\langle T_a(-1), T_a(-\tau)\rangle + (1 - d^*)\langle T_o(-1), T_a(-\tau)\rangle \\ \langle T_o(0), T_o(-\tau)\rangle = c^*\langle T_a(-1), T_o(-\tau)\rangle + (1 - d^*)\langle T_o(-1), T_o(-\tau)\rangle, \end{cases}$$

where $\tau > 1$. In the midlatitudes covariance at lags -2 and -3 were used, while covariance at lags -1 and -2 were used in the subtropics. The covariance at closer lags cannot be used for this estimation in order to minimize the uncertainty due to the persistence of forcing.

In Table 2, the estimated parameters are shown for both the GCM and the observation in the subtropics

TABLE A1. AMIP-to-COUP variance ratios using the results from GCM for the North Pacific and extended linear model simulations. To be used as forcing for the extended linear model, the one-month-lead forecast by the linear model is subtracted from the coupled GCM simulation and forms the whole residuals (R_a and R_o). For the case without Ekman advection, the forcing is obtained by subtracting the Ekman advection from the whole residual. The Ekman layer is assumed equivalent to the mixed layer thickness.

$\frac{\sigma^2(T^M)}{\sigma^2(T^C)}$	Midlatitudes	Subtropics
GCM simulations	1.09	0.79
Linear model with the whole residuals	1.04	0.80
Linear model without Ekman	0.88	0.74

(25°–35°N, 160°E–180°) and midlatitudes (35°–45°N, 180°–220°E) of the North Pacific. Compared to the observation, the GCM indicates weaker stability in the midlatitudes, with $\hat{z} = 1.57$, and stronger stability in the subtropics, with $\hat{z} = 2.17$. Compared to BB98's case, the stability appears to be quite weak, mainly due to a less negative atmospheric response parameter $b(b \gg 0.5)$. Overall, the parameters estimated from our GCM and the observations imply that the coupled system can be excited by forcing more easily in the midlatitudes with stronger coupling than in the subtropics. It is also indicated that GCM or observed coupled system is better represented by BB98's parameters in the subtropics than in the midlatitudes.

To validate the linear model, the area-averaged GCM temperatures for the both COUP and ensemble mean AMIP are reproduced using the linear model with the residual of both air temperature and SST as forcing. For the residual estimation, the difference was taken from each month between the actual data and the linear model ran for one month starting from the previous month. Then, the Ekman advection from GCM was averaged between the previous and the current months to represent the forcing between the two months. For the case of whole forcing, the whole residuals are used to simulate both air temperature (R_a) and SST (R_o). Then, response air temperature is simulated using the SST. The response-to-coupled variance ratio obtained from the GCM results is well reproduced by the case of whole residual forcing, both in the midlatitudes and subtropics. For the case without Ekman advection, we subtract Ekman advection from the residual of SST and use it as the forcing, while the air temperature is forced by the whole residual. The response air temperature is calculated using the SST driven without Ekman advection. It is indicated that the response variance would no longer exceed the coupled variance if there was no Ekman advection. It is also found that the ratio substantially decreases from 1.08 to 0.8 without Ekman advection, which is a 15% reduction in the midlatitudes. In the subtropics, only an 8% reduction in the response-to-coupled ratio is estimated (Table A1).

REFERENCES

Alexander, M. A., and C. Deser, 1995: A mechanism for the recurrence of wintertime midlatitude SST anomalies. *J. Phys. Oceanogr.,* **25,** 122–137.

——, and J. D. Scott, 1997: Surface flux variability over the North Pacific and North Atlantic Oceans. *J. Climate,* **10,** 2963–2978.

——, I. Bladé, M. Newman, J. R. Lanzante, N.-C. Lau, and J. D. Scott, 2002: The atmospheric bridge: The influence of ENSO teleconnections on air–sea interaction over the global oceans. *J. Climate,* **15,** 2205–2231.

Barsugli, J. J., 1995: Idealized models of intrinsic midlatitude atmosphere–ocean interaction. Ph.D. dissertation, University of Washington, 189 pp.

——, and D. S. Battisti, 1998: The basic effects of atmosphere–ocean thermal coupling on midlatitude variability. *J. Atmos. Sci.,* **55,** 477–493.

Battisti, D. S., U. S. Bhatt, and M. A. Alexander, 1995: A modeling study of the interannual variability of sea surface temperature in the wintertime North Atlantic Ocean. *J. Climate,* **8,** 3067–3083.

Bhatt, U. S., M. A. Alexander, D. S. Battisti, D. D. Houghton, and L. M. Keller, 1998: Atmosphere–ocean interaction in the North Atlantic: Near-surface climate variability. *J. Climate,* **11,** 1615–1632.

Bladé, I., 1997: The influence of midlatitude ocean–atmosphere coupling on the low-frequency variability of a GCM. Part I: No tropical SST forcing. *J. Climate,* **10,** 2087–2106.

——, 1999: The influence of midlatitude ocean–atmosphere coupling on the low-frequency variability of a GCM. Part II: Interannual variability induced by tropical SST forcing. *J. Climate,* **12,** 21–45.

Bretherton, C. S., and D. S. Battisti, 2000: An interpretation of the results from atmospheric general circulation models forced by the time history of the observed sea surface temperature distribution. *Geophys. Res. Lett.,* **27,** 767–770.

Cayan, D., 1992: Variability of latent and sensible heat fluxes estimated using bulk formulae. *Atmos.–Ocean,* **30,** 1–42.

Czaja, A., 2003: On the time variability of the net ocean-to-atmosphere heat flux in midlatitudes, with application to the North Atlantic basin. *Quart. J. Roy. Meteor. Soc.,* **129,** 2867–2878.

——, A. Robertson, and T. Huck, 2003: The role of Atlantic Ocean–atmosphere coupling in affecting North Atlantic Oscillation. *The North Atlantic Oscillation: Climatic Significance and Environmental Impact, Geophys. Monogr.,* Vol. 134, Amer. Geophys. Union, 147–172. [Available online at http://www.sp.ph.ic.ac.uk/~arnaud/PAPER/AGU_NAO_chap7.pdf.]

Da Silva, A., C. Young, and S. Levitus, 1994: *Atlas of Surface Marine Data 1994.* Vol. 3, *Anomalies of Heat and Momentum Fluxes,* Department of Commerce, 413 pp.

Davis, R. E., 1976: Predictability of sea surface temperature and sea level pressure anomalies over the North Pacific Ocean. *J. Phys. Oceanogr.,* **6,** 249–266.

Dommenget, D., and M. Latif, 2002: Analysis of observed and simulated SST spectra in the midlatitudes. *Climate Dyn.,* **19,** 277–288.

Frankignoul, C., and K. Hasselman, 1977: Stochastic climate models. Part II: Application to sea surface temperature anomalies and thermocline variability. *Tellus,* **29,** 289–305.

——, and E. Kestenare, 2002: The surface heat flux feedback. Part I: Estimates from observations in the Atlantic and the North Pacific. *Climate Dyn.,* **19,** 633–647.

——, A. Czaja, and B. L'Heveder, 1998: Air–sea feedback in the North Atlantic and surface boundary conditions for ocean models. *J. Climate,* **11,** 2310–2324.

Gates, W. L., 1992: AMIP: The Atmospheric Model Intercomparison Project. PCMDI 7, Lawrence Livermore National Laboratory, 17 pp.

Hall, A., and S. Manabe, 1997: Can local linear stochastic theory explain sea surface temperature and salinity variability? *Climate Dyn.,* **13,** 167–180.

Harzallah, A., and R. Sadourny, 1995: Internal versus SST-forced atmospheric variability as simulated by an atmospheric general circulation model. *J. Climate,* **8,** 474–495.

Jacob, R. L., 1997: Low frequency variability in the simulated atmosphere–ocean system. Ph.D. thesis, University of Wisconsin—Madison, 155 pp.

Kang, I.-S., J.-Y. Lee, and C.-K. Park, 2004: Potential predictability of summer mean precipitation in a dynamical seasonal prediction system with systematic error correction. *J. Climate,* **17,** 834–844.

Kushnir, Y., W. A. Robinson, I. Bladé, N. M. J. Hall, S. Peng, and R. Sutton, 2002: Atmospheric GCM response to extratropical SST anomalies: Synthesis and evaluation. *J. Climate,* **15,** 2233–2256.

Lee, D. E., 2006: The impact of Ekman advection on the North Pacific coupled climate variability. Ph.D. thesis, University of Wisconsin—Madison, 162 pp.

——, and Z. Liu, 2004: An assessment of the contribution of Ekman transport to ocean–atmosphere feedback in the midlatitude North Pacific. *CLIVAR Exchanges,* No. 28, International CLIVAR Project Office, Southampton, United Kingdom.

Liu, Z., 1993: Interannual positive feedbacks in a simple extratropical air–sea coupling system. *J. Atmos. Sci.,* **50,** 3022–3028.

——, and L. Wu, 2004: Atmospheric response to North Pacific SST: The role of ocean–atmosphere coupling. *J. Climate,* **17,** 1859–1882.

Manabe, S., and R. J. Stouffer, 1996: Low-frequency variability of surface air temperature in a 1000-year integration of a coupled atmosphere–ocean–land surface model. *J. Climate,* **9,** 376–393.

Mehta, V. M., M. J. Suarez, J. V. Manganello, and T. L. Delworth, 2000: Oceanic influence on the North Atlantic Oscillation and associated Northern Hemisphere climate variations: 1959–1993. *Geophys. Res. Lett.,* **27,** 121–124.

Namias, J., 1965: Macroscopic association between mean monthly sea surface temperature and the overlying winds. *J. Geophys. Res.,* **70,** 2307–2318.

Norris, J. R., Y. Zhang, and J. Wallace, 1998: Role of low clouds in summertime atmosphere–ocean interactions over the North Pacific. *J. Climate,* **11,** 2482–2490.

Peng, S., and J. S. Whitaker, 1999: Mechanisms determining the atmospheric response to midlatitude SST anomalies. *J. Climate,* **12,** 1393–1408.

Penland, C., and P. D. Sardeshmukh, 1995: The optimal growth of tropical sea surface temperature anomalies. *J. Climate,* **8,** 1999–2024.

——, and L. Matrosova, 1998: Prediction of tropical Atlantic sea surface temperatures using linear inverse modeling. *J. Climate,* **11,** 483–496.

Pierce, D. W., T. P. Barnett, N. Schneider, R. Saravanan, D. Dommenget, and M. Latif, 2001: The role of ocean dynamics in producing decadal climate variability in the North Pacific. *Climate Dyn.,* **18,** 51–70.

Rodwell, M. J., D. P. Rowell, and C. K. Folland, 1999: Oceanic forcing of the wintertime North Atlantic Oscillation and European climate. *Nature,* **398,** 320–323.

Rowell, D. P., 1998: Assessing potential seasonal predictability with an ensemble of multidecadal GCM simulations. *J. Climate,* **11,** 109–120.

Saravanan, R., 1998: Atmospheric low-frequency variability and its relationship to midlatitude SST variability: Studies using the NCAR Climate System Model. *J. Climate,* **11,** 1386–1404.

——, and J. C. McWilliams, 1998: Advective ocean–atmosphere interaction: An analytical stochastic model with implications for decadal variability. *J. Climate,* **11,** 165–188.

——, and P. Chang, 1999: Oceanic mixed layer feedback and tropical Atlantic variability. *Geophys. Res. Lett.,* **26,** 3629–3632.

Schneider, N., A. J. Miller, and D. W. Pierce, 2002: Anatomy of North Pacific decadal variability. *J. Climate,* **15,** 586–605.

Seager, R., Y. Kushnir, N. H. Naik, M. A. Cane, and J. Miller, 2001: Wind-driven shifts in the latitude of the Kuroshio–Oyashio Extension and generation of SST anomalies on decadal timescales. *J. Climate,* **14,** 4249–4265.

Smith, S. D., 1988: Coefficients for sea surface wind stress, heat flux, and wind profiles as a function of wind speed and temperature. *J. Geophys. Res.,* **93,** 15 467–15 472.

Sura, P., M. Newman, and M. A. Alexander, 2006: Daily to decadal sea surface temperature variability driven by state-dependent stochastic heat fluxes. *J. Phys. Oceanogr.,* **36,** 1940–1958.

Sutton, R., and P. P. Mathieu, 2002: Response of the atmosphere–ocean mixed-layer system to anomalous ocean heat-flux convergence. *Quart. J. Roy. Meteor. Soc.,* **128,** 1259–1275.

Winkler, C. R., M. Newman, and P. D. Sardeshmukh, 2001: A linear model of wintertime low-frequency variability. Part I: Formulation and forecast skill. *J. Climate,* **14,** 4474–4494.

Wu, L., Z. Liu, R. Gallimore, R. Jacob, D. E. Lee, and Y. Zhong, 2003: Pacific decadal variability: The tropical Pacific mode and the North Pacific mode. *J. Climate,* **16,** 1101–1120.

Yulaeva, E., N. Schneider, D. W. Pierce, and T. P. Barnett, 2001: Modeling of North Pacific climate variability forced by oceanic heat flux anomalies. *J. Climate,* **14,** 4027–4046.